East Asian summer monsoon climates and cave hydrological cycles over Dansgaard-Oeschger events 14 to 11 revealed by a new stalagmite record from Hulu Cave

Yijia Liang^{a,b}, Yongjin Wang^{a,b*}, Quan Wang^{a,b,c}, Jiangying Wu^{a,b}, Qingfeng Shao^{a,b}, Zhenqiu Zhang^{a,b,d}, Shaohua Yang^{a,b}, Xinggong Kong^{a,b}, R. Lawrence Edwards^{a,e}

(RECEIVED September 22, 2018; ACCEPTED June 11, 2019)

Abstract

A 230 Th/U-dated stalagmite from Hulu Cave was analyzed for $\delta^{18}O$, $\delta^{13}C$, and trace elements. A ^{18}O record, spanning 51.7–42.6 ka, revealed Dansgaard-Oeschger (DO) events 14 to 11. A similar rapid transition and synchronous timing of the onset of DO 12 is evident between the Greenland and Hulu Cave records, which suggests a common forcing mechanism of DO cycles in the North Atlantic and monsoonal region of Asia. Centennial-scale monsoonal oscillations in the cave $\delta^{18}O$ record are indicative of hydroclimatic instability during interstadials. After removing the signals of remote moisture sources, the proportion of moisture from nearby sources is found to be higher during stadials than during interstadials. To explain this, we propose that the movement of the westerly jet is an important control on the balance of nearby and distant moisture sources in East Asia. In addition, the records of $\delta^{13}C$ and trace element ratios, which are proxies of local environmental changes, resemble the $\delta^{18}O$ record on the scale of DO cycles, as well as on even shorter timescales. This suggests that hydrological processes and biological activity at the cave site respond sensitively to the monsoonal changes.

Keywords: Hulu Cave; Stalagmite; East Asian summer monsoon; Dansgaard-Oeschger events; Cave hydrological cycles

INTRODUCTION

During the last glacial period, roughly 120–10 ka, high-amplitude, relatively short-duration climatic oscillations are evident in Greenland ice-core records (Johnsen et al., 1992; Dansgaard et al., 1993; Andersen et al., 2004). These so-called Dansgaard-Oeschger (DO) events were rapid, decadal-scale transitions from cold conditions (Greenland stadials, GS) to warm conditions (Greenland interstadials, GI), followed by a slow return to cold stadial conditions, within an interval of centuries to millennia (Wolff et al., 2010). In addition to Greenland ice cores, DO cycles have been observed in numerous geological archives in the

Cite this article: Liang, Y., Wang, Y., Wang, Q., Wu, J., Shao, Q., Zhang, Z., Yang, S., Kong, X., Edwards, R. L. 2019. East Asian summer monsoon climates and cave hydrological cycles over Dansgaard-Oeschger events 14 to 11 revealed by a new stalagmite record from Hulu Cave. *Quaternary Research* 1–13. https://doi.org/10.1017/qua.2019.39

Northern Hemisphere, including terrestrial and marine sediments (Wang et al., 2001; Voelker, 2002; Deplazes et al., 2013; Rousseau et al., 2017).

The character of DO events in Chinese cave deposits differs from, and is more complex than, paleoclimatic records from northern, high latitudes. An annually laminated stalagmite record from northern China resembles the Greenland NGRIP (the North Greenland Ice Core Project) ice-core record in terms of the timing and duration of the abrupt transitions into DO 15.2 and 14 (Duan et al., 2016). The onset of DO 12, however, is extended in stalagmite records from two caves in southwestern China, lasting from one to several millennia (Cai et al., 2006; Han et al., 2016). These regional differences may result from somewhat different forcing mechanisms. In northern China, monsoon climates are dominated by temperature changes in high, northern latitudes mediated via the westerlies (Duan et al., 2016). Climates in southwestern China, however, are controlled by crossequatorial airflows and temperature changes in the Southern

^aSchool of Geography, Nanjing Normal University, Nanjing 210023, China

^bKey Laboratory of Virtual Geographic Environment, Nanjing Normal University, Ministry of Education, Nanjing 210023, China

^cSchool of Geography and Tourism, Chongqing Normal University, Chongqing 401331, China

dSchool of Life Sciences, Nanjing Normal University, Nanjing 210023, China

^eDepartment of Earth Sciences, University of Minnesota, Minnesota 55455, USA

^{*}Corresponding author. e-mail address: yjwang@njnu.edu.cn (Y. Wang).

Hemisphere (Cai et al., 2006; An et al., 2015). In addition, statistical analysis of a single paleoclimatic record from Hulu Cave in eastern China showed that both Northern and Southern Hemisphere climates affected the pattern of monsoonal DO events, with different ratios of southern and northern climate signals evident (Rohling et al., 2009). Indeed, paleoclimatic records from caves have been regarded as correlating either with temperature changes in Greenland (Wang et al., 2001, 2008; Burns et al., 2003; Zhao et al., 2010; Deplazes et al., 2013) or in Antarctica (Cai et al., 2006; Chen et al., 2016; Han et al., 2016) on the millennial scale. Thus, further analysis of speleothem records from Hulu Cave can potentially provide insights into the regional nature of DO signals, since the site was likely influenced in part by moisture from the Indian monsoon subsystem during the last ice age (Pausata et al., 2011). In addition, due to the sparsity of high-resolution speleothem records, little evidence is available to conduct a detailed analysis of monsoon climates on the centennial scale during Marine Oxygen Isotope Stage (MIS) 3.

Whereas the broad anti-correlation between rainfall somewhere in the monsoon system and speleothem δ^{18} O from Chinese caves is generally accepted, the specifics are controversial. Several studies have interpreted such records as resulting from differential Rayleigh fractionation of water vapor between tropical moisture sources and cave sites and/or changes in the seasonal duration or intensity of monsoon rainfall (perhaps related to the seasonal position of the subtropical jet), a set of processes often referred to as "monsoon intensity" (Wang et al., 2001; Cai et al., 2006, 2010; Kelly et al., 2006; Duan et al., 2015; Orland et al., 2015; Tan et al., 2017, 2018). The extent to which these processes correlate with rainfall amount has been confirmed in some localities through independent quantitative lake-level records of past rainfall variability (Zhang et al., 2011; Goldsmith et al., 2017). A study of the ¹⁰Be record of Chinese loess deposits, a proxy of summer monsoon rainfall, suggested that orbital-scale monsoonal changes were also forced by differences in the proportions of moisture from Indian and East Asian monsoon sources (Beck et al., 2018). This argument is consistent with some climate model simulations and interpretations based upon atmospheric reanalysis data (Maher, 2008; Dayem et al., 2010; Wu et al., 2015). In the present study, we developed a new strategy for determining how the proportions of water vapor derived from remote and nearby sources affect speleothem δ^{18} O records from China.

Proxies such as $\delta^{13}C$ and trace element content of speleothems are effective indicators of palaeohydrological conditions under appropriate circumstances (Fairchild and Treble, 2009 and references therein). However, compared to $\delta^{18}O$ records, they have been underutilized in paleoenvironmental studies of speleothems in China. Nevertheless, in a specific cave environment, $\delta^{13}C$ and trace elements can be applied as hydrological tracers at a local scale (Genty et al., 2003; Sinclair et al., 2012; Huang et al., 2016; Zhao et al., 2016; Wang et al., 2018). Moreover, a relationship between $\delta^{13}C$ and trace element ratios in speleothems has been observed; for

example, owing to the impact of prior calcite precipitation (PCP) and CO₂ degassing under low-flow conditions, metal/Ca ratios and δ^{13} C are elevated in dripwater and hence in stalagmites (Treble et al., 2003; Johnson et al., 2006; Fairchild and Treble, 2009; Stoll et al., 2012; Chen and Li, 2018). Trace element enrichment can also be associated with warm and humid climatic conditions due to enhanced chemical weathering, and thus it reflects local hydrological dynamics (Borsato et al., 2007; Zhou et al., 2008). Hellstrom and McCulloch (2000) showed that concentrations of Sr and Ba in speleothems were positively correlated with changes in the overlying vegetation cover, which confirms the effectiveness of carbon isotopes and trace elements for reconstructing local environmental changes. A recent study of a 3000-yr annually laminated stalagmite from Hulu Cave demonstrated the covariation of records of δ¹⁸O and Sr/Ca ratio on centennial to multi-decadal scales, which enabled the authors to interpret the δ^{18} O record in terms of the monsoonal rainfall (Duan et al., 2015).

In this context, we conducted a multi-proxy study of a new 230 Th/U-dated stalagmite from Hulu Cave (HL161), spanning the interval of 51.7–42.6 ka (relative to the present, defined as AD 1950). The δ^{18} O record has an average resolution of \sim 10 yr, which enables us to identify fine-scale monsoonal variations during DO cycles 14–11. Our study has three aims: (1) to determine the timing and structure of the monsoonal response to DO events; (2) to reconstruct local hydrological processes; and (3) to provide a better understanding of the origin of speleothem δ^{18} O records from caves in China.

SITE, MATERIALS AND METHODS

Stalagmite sample HL161 was found in a naturally detached state on the northern slope in Hulu Cave, Nanjing, in eastern China (32°30′N, 119°10′E, 86 m above sea level). A detailed site description is given in Wang et al. (2001) and Duan et al. (2015). The stalagmite, which has a length of 243 mm and an asymmetric shape, was sliced along its growth axis and polished; no depositional hiatuses are evident (Fig. 1).

For ²³⁰Th/U dating, 15 subsamples of up to 100 mg were extracted using a 0.9-mm-diameter carbide dental drill. The procedures used for U/Th chemical separation and isotopic measurements are detailed in Shao et al. (2017). The carbonate samples were weighed and dissolved in 7N HNO₃ in Teflon beakers containing a known quantity of a ²²⁹Th-²³³U-²³⁶U triple spike. U and Th were preconcentrated by coprecipitation with iron hydroxide and then separated from each other and from other cations by passing the sample solution through a U-TEVA resin column. The U/Th fractions were then dried and diluted in a mixture of 0.1N HNO3 and 0.01N HF for isotopic analysis by a multi-collector inductively coupled plasma mass spectrometer (MC-ICP-MS, Neptune) at the School of Geography, Nanjing Normal University, using the methods described in Shao et al. (2019). The U isotopic data were acquired by two static sequences. The first sequence measured ²³³U, ²³⁵U, ²³⁶U, and ²³⁸U in Faraday cups and simultaneously ²³⁴U on the secondary

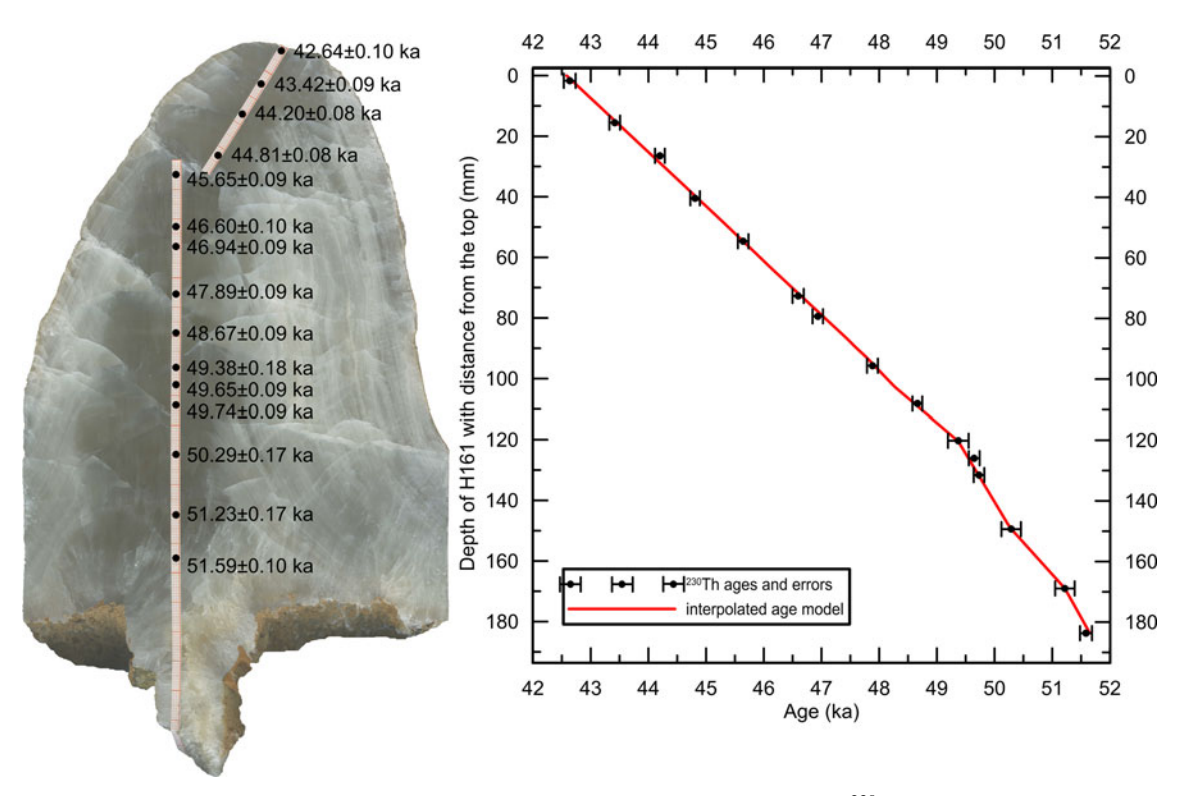


Figure 1. (Color online) Chronology of stalagmite HL161. (a) Scanned image and location of fifteen ²³⁰Th samples. (b) The linearly-interpolated age model, including error bars for ²³⁰Th ages.

electron multiplier (SEM); and the second sequence measured ²³⁶U on the SEM and the other isotopes are in Faraday cups. Thorium measurements were carried out immediately after U measurements for the same sample. The ²²⁹Th and ²³⁰Th were alternately measured on the SEM and ²³²Th in a Faraday cup. Mass fractionation was corrected by comparing the measured ²³⁸U/²³⁵U to the natural value of 137.760 for HU-1 and 137.818 for unknown samples (Hiess et al.,

2012). Hydride interferences, machine abundance sensitivity, and amplifier gains were evaluated every day prior to measurements. 230 Th/U ages were calculated using half-lives of 75,584 yr and 245,620 yr for 230 Th and 234 U, respectively (Cheng et al., 2013). The 230 Th/U age uncertainty was estimated by Monte-Carlo simulations (n = 10^6). All of the speleothem ages have 2-sigma analytical errors of roughly 0.2–0.4% (Table 1).

Table 1. ²³⁰Th dating results for sample HL161 stalagmite from Hulu Cave, China.

Sample number	Depth (mm)	²³⁸ U (ppb)	²³² Th (ppt)	δ^{234} U (measured)	[²³⁰ Th/ ²³⁸ U] (activity)	[²³⁰ Th/ ²³² Th] (activity)	Age (ka; uncorrected)	Age (ka; corrected)
HL161-1	1	247.78 ± 0.24	636.18 ± 0.70	2162.2 ± 2.0	1.0661 ± 0.0021	>1270	42.72 ± 0.10	42.64 ± 0.10
HL161-2	15.5	155.59 ± 0.04	133.42 ± 0.21	2159.7 ± 2.3	1.0816 ± 0.0019	>3850	43.49 ± 0.09	43.42 ± 0.09
HL161-3	26.5	317.35 ± 0.14	69.98 ± 0.15	2264.0 ± 2.6	1.1349 ± 0.0016	>15,660	44.27 ± 0.08	44.20 ± 0.08
HL161-4	40.5	230.08 ± 0.07	781.59 ± 0.82	2256.3 ± 2.1	1.1460 ± 0.0016	>1030	44.90 ± 0.08	44.81 ± 0.08
HL161-5	55	258.37 ± 0.01	59.16 ± 0.16	2279.3 ± 2.4	1.1718 ± 0.0018	>15,600	45.71 ± 0.09	45.65 ± 0.09
HL161-6	73	242.55 ± 0.08	76.88 ± 0.19	2171.0 ± 2.4	1.1523 ± 0.0018	>11,100	46.67 ± 0.10	46.60 ± 0.10
HL161-7	79.5	246.11 ± 0.10	66.65 ± 0.13	2215.1 ± 2.5	1.1758 ± 0.0016	>13,240	47.01 ± 0.09	46.94 ± 0.09
HL161-8	96	275.25 ± 0.12	71.65 ± 0.14	2205.0 ± 2.7	1.1918 ± 0.0017	>13,950	47.95 ± 0.09	47.89 ± 0.09
HL161-9	108.4	205.80 ± 0.08	37.00 ± 0.09	2221.2 ± 2.1	1.2142 ± 0.0016	>20,630	48.73 ± 0.09	48.67 ± 0.09
HL161-10	121	299.72 ± 0.20	39.41 ± 8.19	2200.1 ± 4.5	1.2208 ± 0.0033	>28,370	49.38 ± 0.18	49.38 ± 0.18
HL161-11	126	277.51 ± 0.14	41.21 ± 0.10	2096.8 ± 2.6	1.1860 ± 0.0016	>24,440	49.72 ± 0.09	49.65 ± 0.09
HL161-12	133	218.53 ± 0.08	43.98 ± 0.10	2187.0 ± 2.5	1.2230 ± 0.0016	>18,560	49.80 ± 0.09	49.74 ± 0.09
HL161-13	150	276.57 ± 0.20	29.16 ± 9.46	2236.9 ± 4.6	1.2541 ± 0.0030	>36,370	50.29 ± 0.17	50.29 ± 0.17
HL161-14	170	344.07 ± 0.26	56.96 ± 10.38	2149.2 ± 5.3	1.2381 ± 0.0026	>22,860	51.23 ± 0.17	51.23 ± 0.17
HL161-15	185	465.94 ± 0.32	410.85 ± 0.38	2320.6 ± 3.5	1.3148 ± 0.0016	>4560	51.67 ± 0.10	51.59 ± 0.10

^{*}Errors are 2-sigma analytical errors. Decay constant values are $\lambda_{230} = 9.1705 \times 10^{-6} \text{ yr}^{-1}$, $\lambda_{234} = 2.82206 \times 10^{-6} \text{ yr}^{-1}$, $\lambda_{238} = 1.55125 \times 10^{-10} \text{ yr}^{-1}$. Corrected 230 Th ages (ka before AD 1950) assume an initial 230 Th/ 232 Th atomic ratio of $(4.4 \pm 2.2) \times 10^{-6}$.

Only the section from the top to 187-mm depth was used for stable isotope analyses, because the lower part was less densely crystallized. Powdered subsamples (each ~50 µg) were shaved at a resolution of 0.1 mm from along the growth axis with a knife. Every second sample (n = 969) was measured using a Finnigan-MAT 253 mass spectrometer coupled with a Kiel Carbonate Device at the School of Geography, Nanjing Normal University, China. All results are reported in parts per mil (‰) relative to the Vienna Pee Dee Belemnite. Repeated analyses of an international standard (NBS19) indicated long-term reproducibility, with precisions better than 0.06% for δ^{18} O and 0.05% for δ^{13} C at the 1-sigma level.

A total of 170 powdered samples were drilled with carbide dental burrs along the growth axis and used for trace element analyses at Chongqing Key Laboratory of Karst Environment, Southwest University, China. Each sample weighed 300 ± 50 μg and was dissolved in a solution of 3% HNO₃ and 1% HF. Mg and Ca were analyzed using an inductively coupled plasma optical emission spectrometer (ICP-OES, Perkin-Elmer), and Sr and Ba were measured using a single-collector inductively coupled plasma mass spectrometer (SC-ICP-MS, Element XR). International standard SLRS-5 was used to determine the accuracy and precision of the analyses. The precisions are better than 3% for Ca, 3% for Mg, 5% for Ba, and 10% for Sr.

Trace element analyses of bedrock and dripwater samples were made using an inductively coupled plasma atomic emission spectrometry (ICP-AES, Perkin-Elmer Optima) in the Department of Civil and Structural Engineering, Hongkong Polytechnic University, China. Nine bedrock samples and three dripwater samples were collected from inside the cave. Powdered subsamples (~10 mg) were drilled in the unweathered part of each bedrock sample using carbide dental burrs. The subsamples were then digested with concentrated HNO3 and HClO4 (in a ratio of 4:1) and taken to complete dryness on a hot plate. The water samples were filtered through a Millipore membrane (0.45 µm) to remove fine particles, transferred to a polyethylene bottle, and then acidified with 0.2% HNO₃. Details of the chemical extraction procedures and the ICP-AES analysis are given in Li et al. (1995). Reagent blanks, standard reference materials (NIST 1646a), and sample replicates were used to assess the accuracy and precision of the analyses. The precisions for the measured elements (Mg, Sr, and Ca) are generally <10%.

RESULTS

Chronology

U-Th isotopic compositions and ²³⁰Th ages for stalagmite HL161 are presented in Table 1. Measured ²³⁸U concentrations range from 155–465 ppb and ²³²Th concentrations range from 29–781 ppt. The corrections for initial detrital ²³⁰Th are negligible, as indicated by the high values of the ²³⁰Th/²³²Th activity ratios (>1000). The age model for stalagmite HL161 was constructed by linear interpolation of the ²³⁰Th/U dates (Fig. 1) and the resulting chronology spans the interval of

51.7–42.6 ka, which includes DO 14–11. The average temporal resolution is ~ 10 yr for stable isotopes (δ^{18} O and δ^{13} C) and ~ 50 yr for trace elements (Mg/Ca, Sr/Ca, and Ba/Ca; Fig. 2). Thus, the records are well-suited for determining the paleoen-vironmental evolution of the monsoonal region of China on millennial to centennial scales.

Time series of the proxy records

The stable isotope records vary substantially during the studied period. $\delta^{18}O$ varies from -8.3 to -5.9% (Fig. 2A) and $\delta^{13}C$ from -5.8 to -3.2% (Fig. 2B). Three positive $\delta^{18}O$ excursions, centered at 49.7, 47.5, and 43.4 ka, enable the entire profile to be divided into four negative phases. These four negative $\delta^{18}O$ intervals correspond to GI 14-11 (Wang et al., 2001). Rapid $\delta^{18}O$ shifts (within <100 yr), with amplitudes >1%, mark the onset of GI 13, 12, and 11. The changes in $\delta^{13}C$ exhibit an antiphased relationship with $\delta^{18}O$ on the millennial scale, with ^{13}C enrichment corresponding to ^{18}O depletion. However, this relationship is muted during GI 14, during which a negative period is evident in the $\delta^{13}C$ record, with no corresponding shift in the $\delta^{18}O$ record.

The "Hendy test" and "Replication test" are used to assess whether calcite precipitation is in equilibrium (Hendy, 1971; Dorale and Liu, 2009). The negative correlation between δ^{18} O and δ^{13} C in stalagmite HL161 (R = -0.37, P < 0.01) indicates insignificant kinetic isotopic effects (Hendy, 1971). Moreover, the record strongly resembles the pattern of millennial-scale fluctuations previously recorded from Hulu Cave, within the dating uncertainties (Fig. 2A; Wang et al., 2001; Cheng et al., 2016). Thus, the record passes the "Replication test" (Dorale and Liu, 2009). Under isotopic equilibrium conditions, the δ^{18} O records of the stalagmites of Hulu Cave reliably reflect the δ^{18} O signal of meteoric precipitation. Modern observations of dripwater and rainwater at the cave site support this interpretation (Wang et al., 2018). Following the reasoning of previous studies (Wang et al., 2001, 2008; Liu et al., 2014; Duan et al., 2015; Cheng et al., 2016; Wang et al., 2018), we conclude that the stalagmite δ^{18} O record is a proxy of the East Asian summer monsoon (EASM), with intervals of δ^{18} O depletion representing stronger monsoon. However, stalagmite δ^{18} O records are likely to integrate the effects of complex hydroclimatic processes, including moisture sources, degree of Rayleigh fractionation, and seasonal duration and intensity of monsoon rainfall.

The concentrations of Mg, Sr, and Ba of stalagmite HL161 are expressed as ratios to Ca. The Mg/Ca, Sr/Ca and Ba/Ca ratios have the following ranges: 3.4×10^{-3} to 8×10^{-3} , 0.1×10^{-3} to 0.4×10^{-3} , and 0.2×10^{-3} to 0.3×10^{-3} , respectively (Fig. 2C–E). The Sr/Ca and Ba/Ca ratios, in particular, are strongly positively correlated (R = 0.65, n = 170, P < 0.01). The trace element ratios exhibit a coherent pattern of long-term fluctuations (bold lines in Fig. 2C–E): relative stability from the beginning of the record until ~48 ka and then a slight increase followed by an overall decreasing trend until ~42.6 ka. Notably, the trace element ratios exhibit

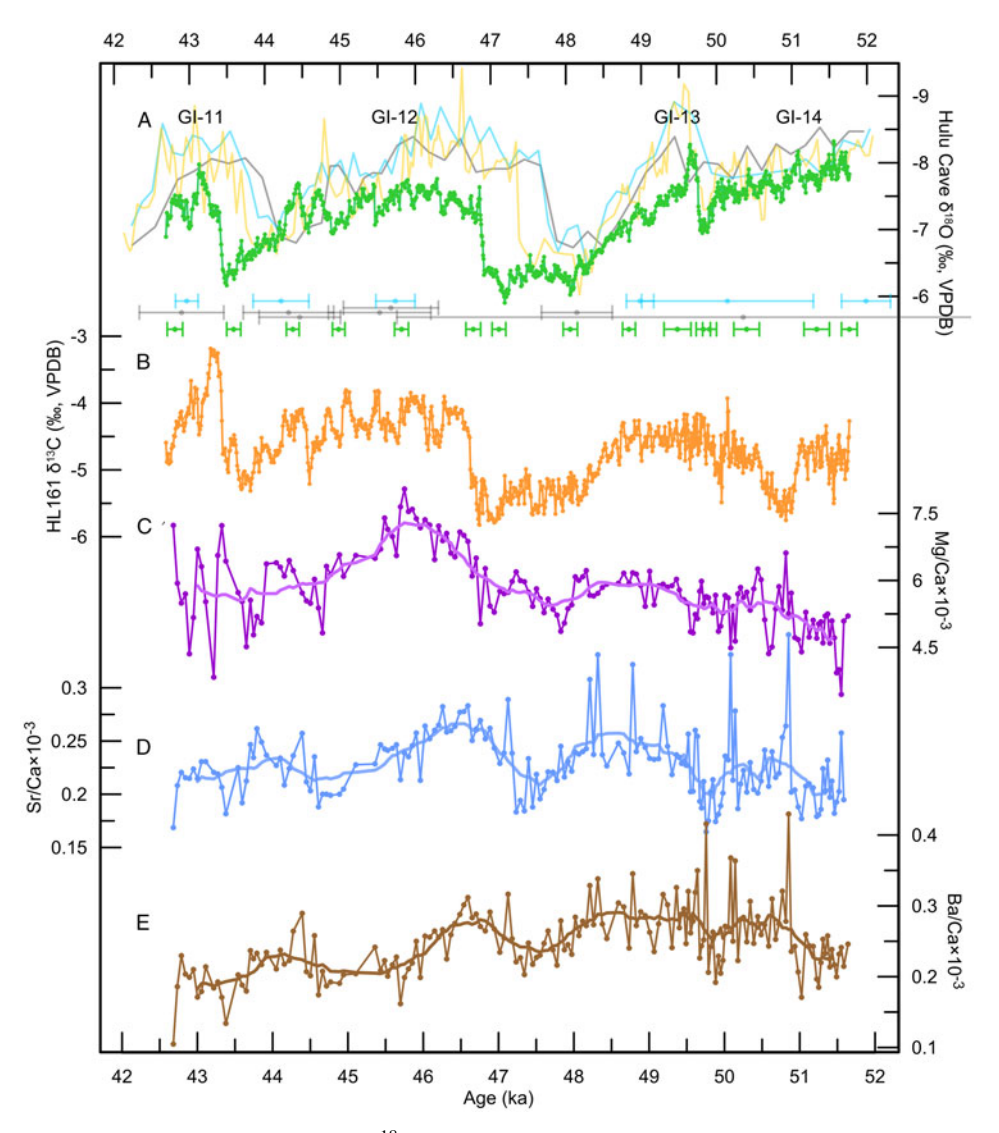


Figure 2. Multi-proxy records for stalagmite HL161. (A) δ^{18} O records for stalagmite HL161 (green curve; this study), MSL (blue curve; Wang et al., 2001), MSD (grey curve; Wang et al., 2001) and a new composite record (yellow curve; Cheng et al., 2016). 2-sigma error bars for the records are also shown with corresponding colors. The previously published Hulu records are plotted for comparison with the record of stalagmite HL161. (B–E) are other multi-proxy records from stalagmite HL161. (B) δ^{13} C. (C) Mg/Ca × 10^{-3} . (D) Sr/Ca × 10^{-3} . (E) Ba/Ca × 10^{-3} . The bold lines in (C–E) are 13-point running averages of the raw data and show the long-term trends. (For interpretation of the references to color in this figure legend, the reader is referred to the web version of this article.)

a long-term pattern of variation similar to that of δ^{13} C, with higher values during GI periods, and vice versa.

DISCUSSION

Climatic teleconnection between the East Asian monsoon and North Atlantic regions

There are striking similarities between the $\delta^{18}O_{calcite}$ record from stalagmite HL161 and the Greenland NGRIP $\delta^{18}O_{ice}$ record (Fig. 3A and B; Andersen et al., 2004). First, a stronger EASM indicated by depleted $\delta^{18}O_{calcite}$ values corresponds closely to Greenland interstadials and vice versa. This millennial-scale coupling of northern, high-latitude climates and low-latitude monsoons has been suggested by several

other studies (Wang et al., 2001; Burns et al., 2003; Carolin et al., 2013; Deplazes et al., 2013; Chen et al., 2016; Kathayat et al., 2016). Second, abrupt monsoonal intensification closely tracks Greenland warming at the start of GI 13, 12, and 11. For example, the onset of GI 12 in the $\delta^{18}O_{calcite}$ record occurs over ~80 yr, which is close to the 60-yr transition of GI 12 in the δ^{18} O_{ice} record, according to Rampfit analysis of both records (Mudelsee, 2000). Third, the duration of GI 12 in the $\delta^{18}O_{calcite}$ record, which lasts ~2600 yr, is approximately equivalent to the duration of GI 12 estimated by Landais et al. (2004) and Wolff et al. (2010). In addition, one centennial-scale warming event which stands out from decadal oscillations in the Greenland $\delta^{18}O_{ice}$ record (referred to as a "rebound event" by Capron et al. [2010]) is also evident in low-latitude hydroclimatic records (dashed line in Fig. 3; see Deplazes et al. [2013]). These comparisons

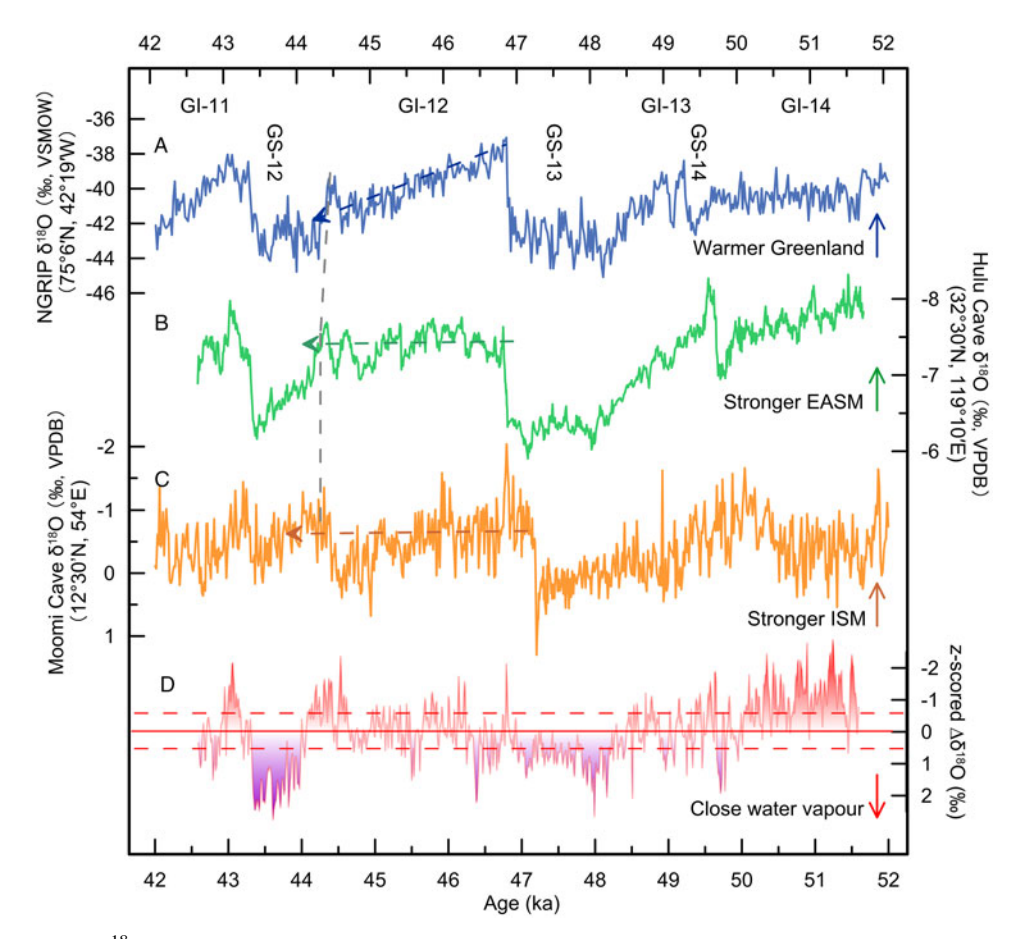


Figure 3. Comparison of δ^{18} O records in the monsoonal regions with Greenland paleotemperature. (A) Greenland NGRIP δ^{18} O_{ice} record (Andersen et al., 2004) plotted on the GICC05 timescale (Svensson et al., 2008). (B) δ^{18} O_{calcite} record from stalagmite HL161 (this study). (C) δ^{18} O_{calcite} record from stalagmite M1-2 (Burns et al., 2003). (D) Reconstructed water vapor source. Δ^{18} O is calculated from the HL161 and M1-2 records and expressed as z-scores. Inferred periods of nearby water vapor sources (z-score Δ^{18} O > 0.53) are shaded with standard deviations denoted by red dashed lines. The grey dashed line indicates a "rebound event" detected in the NGRIP δ^{18} O ice record (Capron et al., 2010). The blue dashed line denotes an overall cooling trend during GI 12, and the green and orange dashed lines indicate stable monsoon climates. (For interpretation of the references to color in this figure legend, the reader is referred to the web version of this article.)

confirm that low-latitude monsoonal strengthening (weakening) corresponds to increased (decreased) Greenland temperature. Potentially, therefore, a common forcing mechanism exists for the DO cycles evident in both the North Atlantic and the Asian monsoonal regions. Potential mechanisms have been suggested to be associated with the Atlantic Meridional Ocean Circulation (Alley et al., 2007) and/or astronomical forcing (Braun et al., 2005).

Previous studies have shown that the GICC05 time scale for Greenland ice cores is systematically too young and that the age offsets increase further back in time (Wang et al., 2001; Fleitmann et al., 2009; Buizert et al., 2014). The age offsets can be explained by the presence of uncertain annual layers (Andersen et al., 2005; Svensson et al., 2008). Comparison with independent, well-dated time makers is an alternative means of evaluating the controversial GICC05 time scale. The onsets of GI 12 and 11 in the record from Hulu Cave are both in excellent agreement with equivalent GI events in the NGRIP record with nominal differences well within dating uncertainties. Our results are in accord with

seven previous studies within dating errors (Burns et al., 2003; Lachniet et al., 2009; Wagner et al., 2010; Carolin et al., 2013; Moseley et al., 2014; Chen et al., 2016; Dong et al., 2018) and thus support the accuracy of the GICC05 time scale within the range of DO 12 and 11.

However, there are noticeable differences in the character of these high- and low-latitude climatic records. For example, during GI 12, Greenland temperature exhibits a decreasing trend (Fig. 3A), while the monsoon remains strong (Fig. 3B and C). In addition, the NGRIP $\delta^{18}O_{ice}$ record is characterized by decadal oscillations (10–50 yr; Boers et al., 2018), which are different from the pattern of centennial monsoonal variability (~250 yr) superimposed on GI events (Fig. 4). This periodicity of monsoon instability approximates that of the de Vries solar cycle (Wagner et al., 2001), which may suggest a sensitive monsoonal response to solar activity under warm climatic conditions (Ji et al., 2005; Wang et al., 2005).

The monsoon system is driven by two primary mechanisms: differential sensible heating between land and sea, and variations in latent heat exported from the southern

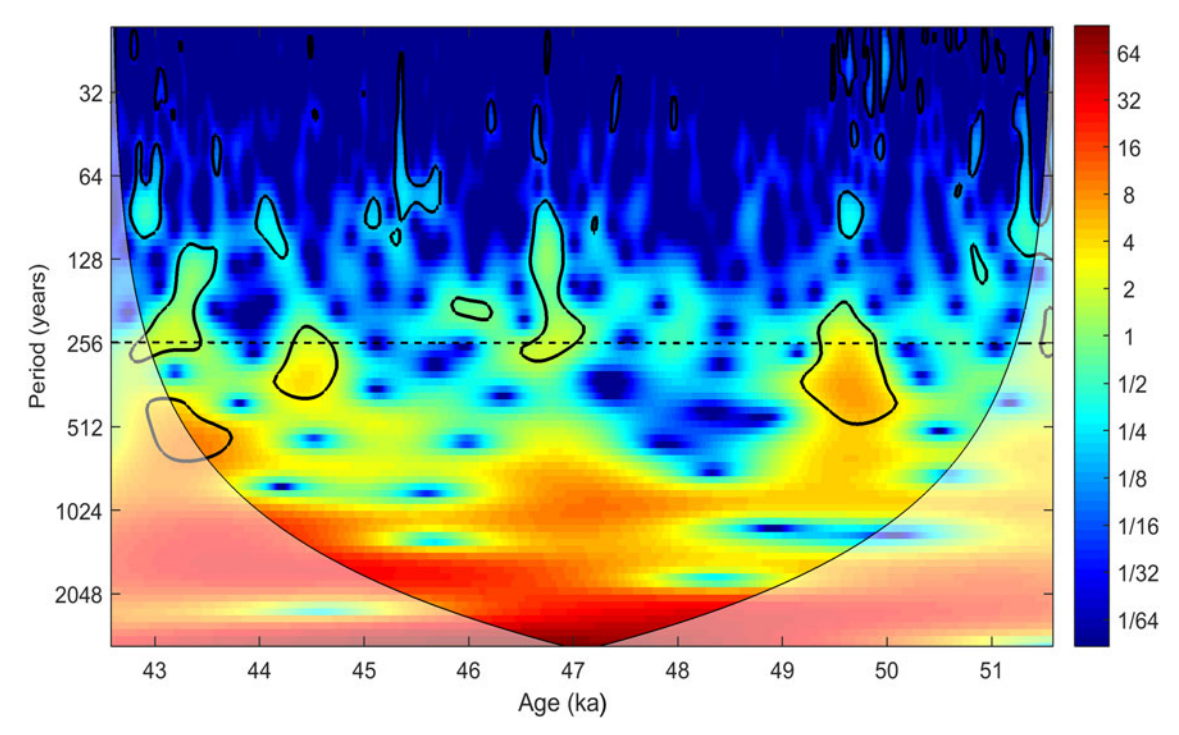


Figure 4. Results of wavelet analysis of the δ^{18} O record from stalagmite HL161. The horizontal dashed line indicates the ~250-yr band prominent during interstadials. Spectral power is shown by colors ranging from deep blue (weak) to deep red (strong). The 95% significance level against red noise is shown by the thick solid line. The spectra were estimated using the method of Grinsted et al. (2004; http://noc.ac.uk/using-science/crosswavelet-wavelet-coherence). (For interpretation of the references to color in this figure legend, the reader is referred to the web version of this article.)

subtropical Indian Ocean via cross-equatorial airflows (An et al., 2015). A temporally variable relationship under different climatic conditions between the EASM and the Northern Hemisphere "pull" factors and Southern Hemisphere "push" factors was determined by Rohling et al. (2009). According to their study, a southern "push" effect has a stronger control on millennial-scale monsoon variability during glacial states, and a northern "pull" effect has a stronger control during deglacial and interglacial states (Rohling et al., 2009). The striking similarity between the NGRIP and HL161 records in terms of their general trends and the abruptness of DO onsets indicates a rapid transmission via an atmospheric "pull" effect. Thus, we suggest that the "push" and "pull" processes affecting the variability of the cave δ^{18} O signals are different between southwestern and eastern/northern China, leading to different DO patterns (Cai et al., 2006; Han et al., 2016; Duan et al., 2016).

Dynamic changes of the westerly jet over China may be an important component of the climatic teleconnection between northern high latitudes and the Asian monsoonal region (Nagashima et al., 2007, 2011; Molnar et al., 2010; Orland et al., 2015). Notably, changes in the timing of the EASM are consistent with the shift of the westerly jet from a location to the south of the Tibetan Plateau to a location to the north (Molnar et al., 2010; Orland et al., 2015). In addition, the jet responds sensitively to northern high-latitude climate, including storm-track movements, sea-ice extent, and sea surface temperature (Laîné et al., 2009). During cold GS phases,

the westerly jet may be weaker and its northward movement is delayed, essentially maintaining East Asia in a prolonged dry pre-monsoonal state (Orland et al., 2015). The southern location of the westerly jet prevents isotopically light water vapor from penetrating into East Asia, resulting in heavier mean $\delta^{18}O$ of rainfall. During the transition from GS to GI climate states, following the abrupt warming in northern high latitudes, a rapid northward movement of the jet may allow rapid and large-scale, low-level monsoonal flow into the interior of East Asia, with a corresponding rapid decrease in $\delta^{18}O_{calcite}$ values. This mechanism is supported by changes in the water vapor supply of EASM rainfall, as discussed below.

The high degree of similarity of the HL161 $\delta^{18}O$ record to other records from Chinese and Indian caves confirms that the $\delta^{18}O$ changes are of regional extent (Burns et al., 2003; Chen et al., 2016; Kathayat et al., 2016; Dong et al., 2018). One possible contributor to $\delta^{18}O$ variability is the water vapor supply from source regions (Dayem et al., 2010; Baker et al., 2015; Wu et al., 2015). In this study, we removed the $\delta^{18}O$ signals of remote water vapor sources from the HL161 record by comparing it with a high-resolution calcite $\delta^{18}O$ record (M1-2) from Moomi Cave in Socotra Island. Socotra Island is located upstream of the EASM - the Indian Ocean (Baker et al., 2015) and is solely influenced by the Indian summer monsoon (Fig. 3C; Burns et al., 2003). The two caves are linked in that they are both under the control of large-scale monsoonal circulation (Wang et al., 2014). According to

the reconstructed global gridded precipitation prediction map of $\delta^{18}O$ (Terzer et al., 2013), the $\delta^{18}O$ values decrease progressively along the pathway of water vapor from Socotra Island (-2.9 to 0.0‰) to South China (-8.9 to -6.0‰). The difference between the average $\delta^{18}O$ values at the two cave sites (6.8%) is well within the range of the $\delta^{18}O$ difference (8.9 to 3.1‰) between the water vapor source (the Indian Ocean) and the site of rainout (Nanjing), which could have been caused by Rayleigh fractionation during transport (Dansgaard, 1964).

Accordingly, we subtracted the M1-2 δ^{18} O record from the HL161 δ^{18} O record, after tuning M1-2 to the HL161 chronology with the aid of the very distinctive GI 12. We then performed a z-score transform (standard deviation = 0.53) and the results are expressed as z-scored $\triangle \delta^{18}$ O (Fig. 3D). The $\Lambda \delta^{18}$ O values represent changes in water vapor supply from relatively close sources, including the West Pacific Ocean and/or inland China. The record enables us to elucidate the control of the westerly jet over the water vapor source of the EASM rainfall (Fig. 3D). Three periods with positive values, centered at 49.7, 47.6, and 43.7 ka and corresponding respectively to GS 14, 13, and 12, are prominent within the record. The positive $\triangle \delta^{18}$ O values represent increased water vapor supply from nearby sources due to the delayed shift in the position of the westerly jet. We then applied Empirical Mode Decomposition (Huang et al., 1998; Huang and Wu, 2008) to determine the water vapor contribution from the Indian Ocean and the West Pacific Ocean/inland China during GS 14 to 12 (excluding the incomplete events GI 14 and 11). The estimated average water vapor proportions derived from distant and sources near Hulu Cave are 56.7 and 43.3%, respectively. However, during GS states, the nearby water vapor source comprises a higher proportion, with values of 47.6, 52.9 and 69.0% for GS 14, 13, and 12, respectively.

Response of cave hydrological cycles to monsoonal changes

The high degree of consistency of the δ^{13} C records from Hulu Cave (Fig. 5A and B) suggests that they reflect a common environmental process (Dorale and Liu, 2009). The antiphased relationship between δ^{13} C and δ^{18} O records of stalagmite HL161 on the millennial scale suggests that δ^{13} C record is sensitive to monsoonal changes (Fig. 2A and B). A possible explanation for this correlation is a "damping model" which reflects local hydrology, with changes linked to rainfall (Kong et al., 2005). A "damping model" requires a specific combination of the conditions of speleothem formation and climate factors: a thin soil cover and elevated precipitation (Baker et al., 1997). Modern field observations show that the site of Hulu Cave has a thin soil cover, <30 cm deep, while rainfall is the main contributor to the recharge of the aquifer above the cave. The aquifer is also highly permeable, which allows rainwater to infiltrate rapidly within a few days after heavy rainfalls. This combination provides the necessary

conditions for the "damping model." Under heavy rainfall, equilibrium between soil water and soil CO_2 cannot be attained due to the short residence time of the water, which results in a low degree of depletion of ^{13}C in the speleothem (Baker et al., 1997; Kong et al., 2005). The inverse process operates under drier and colder climatic conditions. Notably, the similarity of speleothem $\delta^{13}C$ and $\delta^{18}O$ records is also demonstrated during the penultimate glacial period (Wang et al., 2018).

The similarity between the trace element ratios (Fig. 2C–E)

on the millennial scale also suggests that they reflect a common set of local processes. Trends in stalagmite composition are ultimately derived from variations in the seepage water which are primarily controlled by local soil, regolith, and bedrock (Fairchild and Treble, 2009). Processes such as PCP, differential dissolution of calcite and dolomite, selective leaching, and acids in water are potential controls of the trace element composition of speleothems (Fairchild et al., 2000; Hellstrom and McCulloch, 2000; Fairchild and Baker, 2012). Among them, PCP is one of the most-often cited explanations for the covariation of trace elements (Johnson et al., 2006; Fairchild and Treble, 2009; Sinclair et al., 2012; Stoll et al., 2012). Sinclair et al. (2012) presented a mathematical model of PCP and showed that the positive linear correlation between ln(Mg/Ca) versus ln(Sr/Ca) was given by $\frac{Kd_{Sr}-1}{Kd_{Mg}-1}.$ This is a universal property of PCP and can be applied even when there is no prior characterization of the dripwater or host rock (Sinclair et al., 2012). Here, we used this model to calculate the slope of the theoretical PCP gradient in Hulu Cave. At a mean annual cave temperature of ~15°C, the partition coefficients adopted here are $Kd_{Mg} = 0.019$ (Huang and Fairchild, 2001) and $Kd_{Sr} = 0.1$ (Treble et al., 2015). Assuming that the partition coefficients are constant and that PCP is the only process occurring in a closed water-rock system, the theoretical PCP gradient in Hulu Cave will be 0.92. However, the calculated slope for stalagmite HL161 is much smaller (0.21, Fig. 5C), thus indicating minor PCP effects during deposition.

At Hulu Cave, the congruent Ordovician limestone (Wang et al., 2018) indicates the absence of differential dissolution (Fairchild et al., 2000). Selective leaching is also unlikely to occur. Compared with the bedrock mixing line, the concentrations of Sr and Mg relative to Ca in the dripwater and stalagmite are depleted (Fig. 5D; Fairchild and Treble, 2009). Therefore, we exclude these factors as possible mechanisms for the covariation.

Our favored explanation relates to the acid concentrations in the soil water. The evidence for this is the case of Ba, which is a relatively immobile element due to the high cation exchange selectivity of Ba²⁺ (Mcbride, 1994). Biological activity, however, can increase the weathering and leaching of Ba²⁺ by producing more concentrated carbonic acid, hydrogen ions, and organic exudates (Taylor et al., 2009). Under warm and wet conditions, these reactive species are supplied to the infiltrating water by elevated root respiration,

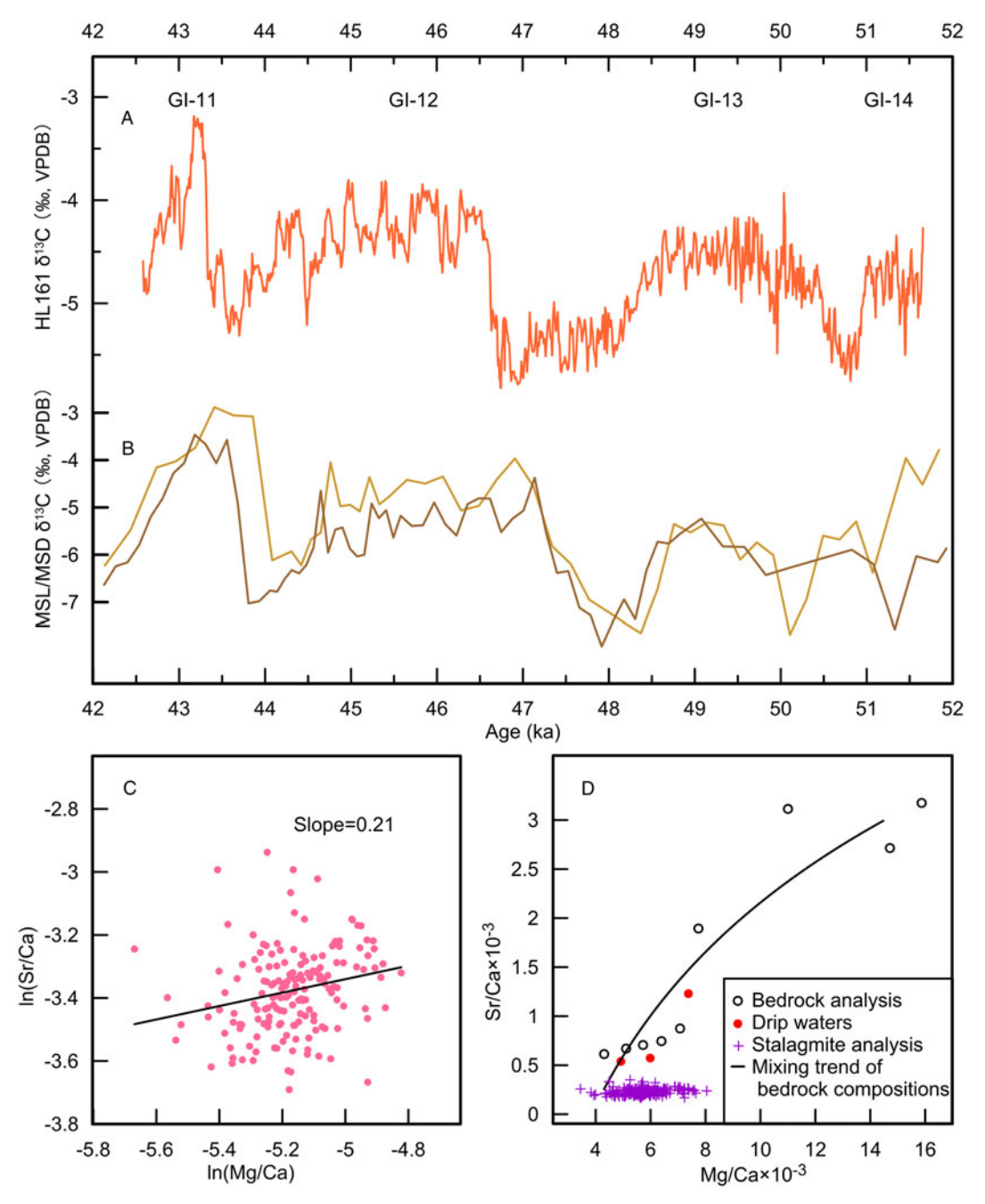


Figure 5. (A and B) Results of a replication test of δ^{13} C records from Hulu Cave. (A) δ^{13} C record for stalagmite HL161. (B) δ^{13} C records from stalagmite MSL (brown) and stalagmite MSD (gold; Kong et al., 2005). (C and D) Results of an analysis of trace element from Hulu Cave. (C) Relationship between ln(Mg/Ca) versus ln(Sr/Ca) for stalagmite HL161 with the slope of the best-fit regression line indicated. (D) Comparison of values of Sr/Ca and Mg/Ca for bedrock (black dots), cave water (red dots), and stalagmite HL161 (purple crosses). The cave water and stalagmite samples are depleted in Mg and Sr relative to Ca in comparison to bedrock. (For interpretation of the references to color in this figure legend, the reader is referred to the web version of this article.)

litter decomposition, and other biological activities (Brook et al., 1983; Taylor et al., 2009; Plestenjak et al., 2012), thus leading to increased concentrations of Ba²⁺ relative to Ca²⁺ (Hellstrom and McCulloch, 2000). The positive correlation between Sr/Ca and Ba/Ca ratios (R = 0.65, n = 170, P < 0.01) and the covariation of their long-term trends suggest that similar processes apply to Sr and Mg. The mobilized cations (Ba, Sr, and Mg) are thereby introduced into the

cave environment from surficial soils and host rock by infiltrating water.

The variations in proxy $\delta^{13}C$ and metal/Ca ratios strongly resemble the HL161 $\delta^{18}O$ record. On the millennial scale, more negative $\delta^{18}O$ values are consistent with the elevated $\delta^{13}C$ values and Mg/Ca, Sr/Ca, and Ba/Ca ratios. This correlation even extends to the centennial scale, such as the episodes of monsoon strengthening at 51.2, 46.5, 45.8, and

44.3 ka. The general agreement between trace element ratios and stable isotope values indicates that both hydrological and biological activity at the local level responded sensitively to changes in monsoon.

CONCLUSIONS

We have produced a high-resolution and 230 Th/U-dated multi-proxy record from a new stalagmite (HL161) from Hulu Cave. The records span the interval of 51.7–42.6 ka that encompasses DO 14–11. The records of the geochemical indicators of δ^{18} O, δ^{13} C, Mg/Ca, Sr/Ca, and Ba/Ca provide new perspectives on the EASM and cave hydrological cycles on millennial to centennial timescales.

The \sim 10-yr-resolution δ^{18} O record is strikingly similar to that of the Greenland ice-core record in terms of the general pattern, suggesting a common forcing factor of DO cycles in both high and low latitudes of the Northern Hemisphere. The rapid transitions at the onset of GI events in our stalagmite record resemble the abrupt DO warming events in the NGRIP record and they are synchronous within dating errors. However, centennial-scale variations (~250 yr) during Chinese interstadials differ from the predominantly decadal-scale (10-50 yr) oscillations in the climate over Greenland. The surprisingly rapid response of the subtropical monsoon to Greenland temperature variations indicates a rapid atmospheric transmission mechanism. After removing the variance associated water vapor from the Indian Ocean from our δ^{18} O record, the proportion of the nearby water vapor sources is higher during GS phases, implying that the westerly jet plays a key role in controlling the water vapor transport to eastern China. Therefore, we conclude that the calcite δ¹⁸O record of Hulu Cave can largely be interpreted as reflecting changes in monsoon intensity, which incorporates changes in water vapor sources.

The $\delta^{13}C$ record of stalagmites from Hulu Cave reflects the effects of a "damping model," which are linked with local rainfall. The Mg/Ca, Sr/Ca, and Ba/Ca ratios of stalagmite HL161 reflect the effects of biological activity within the soil above the cave during water infiltration. On the millennial and even the centennial scale, changes in $\delta^{13}C$ and metal/Ca ratios resemble the $\delta^{18}O$ record, with higher $\delta^{13}C$ and metal/Ca ratios corresponding to lower $\delta^{18}O$ values. This observation indicates that changes in local hydrology and ecosystem respond sensitively to variations in monsoon.

ACKNOWLEDGEMENTS

The authors are grateful to Jeffrey Dorale and two anonymous reviewers for their valuable comments, which substantially improved the manuscript. This research was supported by the National Nature Science Fund of China (awards 41571102, 41672164, 41372174, and 41130210), the Priority Academic Program Development of Jiangsu Higher Education Institutions (award 164320H116), the Jiangsu Center for Collaborative Innovation in Geographical Information Resource development and

Application, the 111 program of China (approved Number: D19002), and United States National Science Foundation Grant 1702816.

REFERENCES

- Alley, R.B., 2007. Wally was right: predictive ability of the North Atlantic "Conveyor Belt" Hypothesis for abrupt climate change. *Annual Review of Earth and Planetary Sciences* 35, 241–272.
- An, Z., Wu, G., Li, J., Sun, Y., Liu, Y., Zhou, W., Cai, Y., et al., 2015. Global monsoon dynamics and climate change. *Journal* of Earth Environment 43, 29–77.
- Andersen, K.K., Azuma, N., Barnola, J.M., Bigler, M., Biscaye, P., Caillon, N., Chappellaz, E., *et al.*, 2004. High-resolution record of Northern Hemisphere climate extending into the last interglacial period. *Nature* 431, 147–151.
- Andersen, K.K., Svensson, A., Johnsen, S., Rasmussen, S.O., Bigler, M., Rothlisberger, R., Ruth, U., *et al.*, 2005. The Greenland ice core chronology 2005, 15–42 ka. Part 1: constructing the time scale. *Quaternary Science Reviews* 25, 3246–3257.
- Baker, A., Ito, E., Smart, P.L., Mcewan, R.F., 1997. Elevated and variable values of δ^{13} C in speleothems in a British cave system. *Chemical Geology* 136, 263–270.
- Baker, A.J., Sodemann, H., Baldini, J.U.L., Breitenbach, S.F.M., Johnson, K.R., van Hunen, J., Zhang, P., 2015. Seasonality of westerly moisture transport in the East Asian summer monsoon and its implications for interpreting precipitation δ¹⁸O. *Journal* of Geophysical Research Atmospheres 120, 5850–5862.
- Beck, J.W., Zhou, W., Li, C., Wu, Z., White, L., Xian, F., Kong, X., et al., 2018. A 550,000-year record of East Asian monsoon rainfall from ¹⁰Be in loess. *Science* 360, 877–881.
- Boers, N., 2018. Early-warning signals for Dansgaard-Oeschger events in a high-resolution ice core record. *Nature Communications* 9, 2556.
- Borsato, A., Frisia, S., Fairchild, I.J., Somogyi, A., Susini, J., 2007. Trace element distribution in annual stalagmite laminae mapped by micrometer-resolution x-ray fluorescence: implications for incorporation of environmentally significant species. *Geochimica et Cosmochimica Acta* 71, 1494–1512.
- Braun, H., Christl, M., Rahmstorf, S., Ganopolski, A., Mangini, A., Kubatzki, C., Roth, K., *et al.*, 2005. Possible solar origin of the 1,470-year glacial climate cycle demonstrated in a coupled model. *Nature* 438, 208–211.
- Brook, G.A., Folkoff, M.E., Box, E.O., 1983. A world model of soil carbon dioxide. *Earth Surface Processes and Landforms* 8, 79–88.
- Buizert, C., Cuffey, K.M., Severinghaus, J.P., Baggenstos, D., Fudge, T.J., Steig, E.J., Markel, B.R., *et al.*, 2014. The WAIS-Divide deep ice core WD2014 chronology-part 2: methane synchronization (68–31 ka BP) and the gas age-ice age difference. *Climate of the Past* 10, 153–173.
- Burns, S.J., Fleitmann, D., Matter, A., Kramers, J., Al-Subbary, A.A., 2003. Indian Ocean climate and an absolute chronology over Dansgaard/Oeschger events 9 to 13. *Science* 301, 1365–1367.
- Cai, Y., An, Z., Cheng, H., Edwards, R.L., Kelly, M.J., Liu, W., Wang, X., et al., 2006. High-resolution absolute-dated Indian monsoon record between 53 and 36 ka from Xiaobailong Cave, southwestern China. Geology 34, 621–624.
- Cai, Y., Tan, L., Cheng, H., An, Z., Edwards, R.L., Kelly, M.J., Kong, X., et al., 2010. The variation of summer monsoon precipitation in central China since the last deglaciation. Earth and Planetary Science Letters 291, 21–31.

- Capron, E., Landais, A., Chappellaz, J., Schilt, A., 2010. Millennial and sub-millennial scale climatic variations recorded in polar ice cores over the last glacial period. *Climate of the Past* 6, 345–365.
- Carolin, S.A., Cobb, K.M., Adkins, J.F., Clark, B., Conroy, J.L., Lejau, S., Malang, J., et al., 2013. Varied response of western pacific hydrology to climate forcings over the last glacial period. Science 340, 1564–1566.
- Chen, C., Li, T., 2018. Geochemical characteristics of cave drip water respond to ENSO based on a 6-year monitoring work in Yangkou cave, southwest China. *Journal of Hydrology* 561, 896–907.
- Chen, S., Wang, Y., Hai, C., Edwards, R.L., Wang, X., Kong, X., Liu, D., 2016. Strong coupling of Asian monsoon and Antarctic climates on sub-orbital timescales. *Scientific Reports* 6, 32995.
- Cheng, H., Edwards, R.L., Shen, C., Polyak, V.J., Asmerom, Y., Woodhead, J., Hellstrom, J., et al., 2013. Improvements in ²³⁰Th dating, ²³⁰Th and ²³⁴U half-life values, and U-Th isotopic measurements by multi-collector inductively coupled plasma mass spectroscopy. Earth and Planetary Science Letters 371–372, 82–91.
- Cheng, H., Edwards, R.L., Sinha, A., Spötl, C., Yi, L., Chen, S., Kelly, M., *et al.*, 2016. The Asian monsoon over the past 640,000 years and ice age terminations. *Nature* 534, 640–646.
- Dansgaard, W., 1964. Stable isotopes in precipitation. *Tellus* 16, 436–468.
- Dansgaard, W., Johnsen, S.J., Clausen, H.B., Dahl-Jensen, D., Gundestrup, N.S., Hammer, C.U., Hvidberg, C.S., et al., 1993. Evidence for general instability of past climate from a 250-kyr ice-core record. *Nature* 364, 218–220.
- Dayem, K.E., Molnar, P., Battisti, D.S., Roe, G. H., 2010. Lessons learned from oxygen isotopes in modern precipitation applied to interpretation of speleothem records of paleoclimate from eastern Asia. *Earth and Planetary Science Letters* 295, 219–230.
- Deplazes, G., Lückge, A., Peterson, L.C., Timmermann, A., Hamann, Y., Hughen, K.A., Röhl, U., et al., 2013. Links between tropical rainfall and North Atlantic climate during the last glacial period. Nature Geoscience 6, 213–217.
- Dong, J., Shen, C., Kong, X., Wang, Y., Duan, F., 2018. Asian monsoon dynamics at Dansgaard/Oeschger events 14–8 and Heinrich events 5–4 in northern China. *Quaternary Geochronol*ogy 47, 72–80.
- Dorale, J.A., Liu, Z., 2009. Limitations of Hendy test criteria in judging the paleoclimatic suitability of speleothems and the need for replication. *Journal of Cave and Karst Studies* 71, 73–80.
- Duan, F., Wu, J., Wang, Y., Edwards, R.L., Cheng, H., Kong, X., Zhang, W., 2015. A 3000-yr annually laminated stalagmite record of the last glacial maximum from Hulu Cave, China. *Quaternary Research* 83, 360–369.
- Duan, W., Cheng, H., Tan, M., Edwards, R.L., 2016. Onset and duration of transitions into Greenland interstadials 15.2 and 14 in northern China constrained by an annually laminated stalagmite. Scientific Reports 6, 20844
- Fairchild, I.J., Baker, A., 2012. Speleothem science: from process to past environments. John Wiley & Sons, Chichester.
- Fairchild, I.J., Borsato, A., Tooth, A.F., Frisia, S., Hawkesworth, C.J., Huang, Y., McDermott, F., et al., 2000. Controls on trace element (Sr–Mg) compositions of carbonate cave waters: implications for speleothem climatic records. Chemical Geology 166, 255–269.
- Fairchild, I.J., Treble, P.C., 2009. Trace elements in speleothems as recorders of environmental change. *Quaternary Science Reviews* 28, 449–468.
- Fleitmann, D., Cheng, H., Badertscher, S., Edwards, R.L., Mudelsee, M., Göktürk, O.M., Fankhauser, A., *et al.*, 2009. Timing and climatic impact of Greenland interstadials recorded in

- stalagmites from northern Turkey. *Geophysical Research Letters* 36, L19707.
- Genty, D., Blamart, D., Ouahdi, R., Gilmour, M., Baker, A., Jouzel, J., Van-Exter, S., 2003. Precise dating of Dansgaard-Oeschger climate oscillations in Western Europe from stalagmite data. *Nature* 421, 833–837.
- Goldsmith, Y., Broecker, W.S., Xu, H., Polissar, P.J., Demenocal, P.B., Porat, N., Lan, J., *et al.*, 2017. Northward extent of East Asian monsoon covaries with intensity on orbital and millennial timescales. *Proceedings of the National Academy of Sciences of the United States of America* 114, 1817–1821.
- Grinsted, A., Moore, J.C., Jevrejeva, S., 2004. Application of the cross wavelet transform and wavelet coherence to geophysical time series. *Nonlinear Processes in Geophysics* 11, 561–566.
- Han, L., Li, T., Cheng, H., Edwards, R.L., Shen, C., Li, H., Huang, C., et al., 2016. Potential influence of temperature changes in the Southern Hemisphere on the evolution of the Asian summer monsoon during the last glacial period. Quaternary International 392, 239–250.
- Hellstrom, J.C., McCulloch, M.T., 2000. Multi-proxy constraints on the climatic significance of trace element records from a New Zealand speleothem. *Earth and Planetary Science Letters* 179, 287–297.
- Hendy, C.H., 1971. The isotopic geochemistry of speleothems I. The calculation of the effects of different modes of formation on the isotopic composition of speleothems and their applicability as palaeoclimatic indicators. *Geochimica et Cosmochimica Acta* 3, 801–824.
- Hiess, J., Condon, D.J., McLean, N., Noble, S.R., 2012. ²³⁸U/²³⁵U Systematics in terrestrial uranium-bearing minerals. *Science* 335, 1610–1614.
- Huang, N., Shen, Z., Long, S., 1998. The empirical mode de-composition and the Hilbert spectrum for nonlinear and nonstationary time series analysis. *Proceedings of the Royal Society A Mathematica* 454, 903–995.
- Huang, N., Wu, Z., 2008. A review on Hilbert-Huang transform: method and its applications to geophysical studies. *Reviews of Geo-physics* 46, RG2006. http://dx.doi.org/10.1029/2007rg000228
- Huang, W., Wang, Y., Cheng, H., Edwards, R.L., Shen, C., Liu, D., Shao, Q., et al., 2016. Multi-scale Holocene Asian monsoon variability deduced from a twin-stalagmite record in southwestern China. Quaternary Research 86, 34–44.
- Huang, Y., Fairchild, I.J., 2001. Partitioning of Sr²⁺ and Mg²⁺ into calcite under karst-analogue experimental conditions. *Geochimica et Cosmochimica Acta* 65, 47–62.
- Ji, J., Shen, J., Balsam, W., Chen, J., Liu, L., Liu, X., 2005. Asian monsoon oscillations in the northeastern Qinghai-Tibet Plateau since the late glacial as interpreted from visible reflectance of Qinghai Lake sediments. *Earth and Planetary Science Letters* 233, 61–70.
- Johnsen, S.J., Clausen, H.B., Dansgaard, W., Fuhrer, K., Gundestrup, N., Hammer, C.U., Iversen, P., et al., 1992. Irregular glacial interstadials recorded in a new Greenland ice core. *Nature* 359, 311–313.
- Johnson, K.R., Hu, C., Belshaw, N.S., Henderson, G.M., 2006. Seasonal trace-element and stable-isotope variations in a Chinese speleothem: the potential for high-resolution paleomonsoon reconstruction. *Earth and Planetary Science Letters* 244, 394–407.
- Kathayat, G., Cheng, H., Sinha, A., Spötl, C., Edwards, R.L., Zhang, H., Li, X., et al., 2016. Indian monsoon variability on millennial-orbital timescales. Scientific Reports 6, 24374.
- Kelly, M., Edwards, R.L., Cheng, H., Yuan, D., Cai, Y., Zhang, M., Lin, Y., *et al.*, 2006. High resolution characterization of the Asian

monsoon between 146,000 and 99,000 years BP from Dongge Cave, China and global correlation of events surrounding termination II. *Palaeogeography Palaeoclimatology Palaeoecology* 236, 20–38.

- Kong, X., Wang, Y., Wu, J., Cheng, H., Edwards, R.L., Wang, X., 2005. Complicated responses of stalagmite δ¹³C to climate change during the last glaciation from Hulu Cave, Nanjing, China. Science in China Series D-Earth Sciences 48, 2174–2181.
- Lachniet, M.S., Johnson, L., Asmerom, Y., Burns, S.J., Polyak, V., Patterson, W. P., Burt, L., et al., 2009. Late quaternary moisture export across Central America and to Greenland: evidence for tropical rainfall variability from Costa Rican stalagmites. Quaternary Science Reviews 28, 3348–3360.
- Laîné, A., Kageyama, M., Salas-Mélia, D., Voldoire, A., Rivière, G., Ramstein, G., Planton, S., et al., 2009. Northern Hemisphere storm tracks during the last glacial maximum in the PMIP2 oceanatmosphere coupled models: energetic study, seasonal cycle, precipitation. Climate Dynamics 32, 593–614.
- Landais, A., Caillon, N., Goujon, C., Grachev, A.M., Barnola, J.M., Chappellaz, J., Jouzel, J., et al., 2004. Quantification of rapid temperature change during DO event 12 and phasing with methane inferred from air isotopic measurements. Earth and Planetary Science Letters 225, 221–232.
- Li, X., Coles, B.J., Ramsey, M.H., Thornton, I., 1995. Sequential extraction of soils for multielement analysis by ICP-AES. *Chemical Geology* 124, 109–123.
- Liu, Z., Wen, X., Brady, E.C., Otto-Bliesner, B., Yu, G., Lu, H., Cheng, H., et al., 2014. Chinese cave records and the East Asia Summer Monsoon. Quaternary Science Reviews 83, 115–128.
- Maher, B.A., 2008. Holocene variability of the East Asian summer monsoon from Chinese cave records: a re-assessment. *Holocene* 18, 861–866.
- McBride, M.B., 1994. *Environmental Chemistry of Soils*. Oxford University Press, New York.
- Molnar, P., Boos, W.R., Battisti, D.S., 2010. Orographic controls on climate and paleoclimate of Asia: Thermal and mechanical roles for the Tibetan Plateau. *Annual Review of Earth and Plane*tary Sciences 38, 77–102.
- Moseley, G.E., Spötl, C., Svensson, A., Cheng, H., Brandstatter, S., Edwards, R.L., 2014. Multi-speleothem record reveals tightly coupled climate between central Europe and Greenland during Marine Isotope Stage 3. *Geology* 42, 1043–1046.
- Mudelsee, M., 2000. Ramp function regression: a tool for quantifying climate transitions. *Computer and Geosciences* 26, 293–307.
- Nagashima, K., Tada, R., Matsui, H., Irino, T., Tani, A., Toyoda, S., 2007. Orbital- and millenial-scale variations in Asian dust transport path to the Japan Sea. *Palaeogeography, Palaeoclimatology, Palaeoecology* 247, 144–161.
- Nagashima, K., Tada, R., Tani, A., Sun, Y., Isozaki, Y., Toyoda, S., Hasegawa, H., 2011. Millennial-scale oscillations of the westerly jet path during the last glacial period. *Journal of Asian Earth Sciences* 40, 1214–1220.
- Orland, I.J., Edwards, R.L., Cheng, H., Kozdon, R., Cross, M., Valley, J.W., 2015. Direct measurements of deglacial monsoon strength in a Chinese stalagmite. *Geology* 43, 555–558.
- Pausata, F.S.R., Battisti, D.S., Nisancioglu, K.H., Bitz, C.M., 2011. Chinese stalagmite $\delta^{18}O$ controlled by changes in the Indian monsoon during a simulated Heinrich event. *Nature Geoscience* 4, 474–480.
- Plestenjak, G., Eler, K., Vodnik, D., Ferlan, M., Čater, M., Kanduč, T., Simončič, P., *et al.*, 2012. Sources of soil CO₂ in

calcareous grassland with woody plant encroachment. *Journal of Soils and Sediments* 12, 1327–1338.

- Rohling, E.J., Liu, Q., Roberts, A.P., Stanford, J.D., Rasmussen, S.O., Langen, P. L., Siddall, M., 2009. Controls on the East Asian monsoon during the last glacial cycle, based on comparison between Hulu Cave and polar ice-core records. *Quaternary Science Reviews* 28, 3291–3302.
- Rousseau, D.D., Svensson, A., Bigler, M., Sima, A., Steffensen, J.P., Boers, N., 2017. Eurasian contribution to the last glacial dust cycles: how are loess sequences built? *Climate* of the Past 13, 1181–1197.
- Shao, Q., Li, C., Huang, M., Liao, Z., Arps, J., Huang, C., Chou, Y., et al., 2019. Interactive programs of MC-ICPMS data processing for ²³⁰Th/U geochronology. *Quaternary Geochronology* 51, 43– 52.
- Shao, Q., Pons-Branchu, E., Zhu, Q., Wang, W., Valladas, H., Fontugne, M., 2017. High precision U/Th dating of the rock paintings at Mt. Huashan, Guangxi, southern China. *Quaternary Research* 88, 1–13.
- Sinclair, D.J., Banner, J. L., Taylor, F.W., Partin, J., Jenson, J., Mylroie, J., Goddard, E., *et al.*, 2012. Magnesium and strontium systematics in tropical speleothems from the western pacific. *Chemical Geology* 294–295, 1–17.
- Stoll, H.M., Müller, W., Prieto, M., 2012. I-STAL, a model for interpretation of Mg/ca, Sr/ca and Ba/ca variations in speleothems and its forward and inverse application on seasonal to millennial scales. *Geochemistry, Geophysics, Geosystems* 13, Q09004, doi:10.1029/2012GC004183.
- Svensson, A., Andersen, K.K., Bigler, M., Clausen, H.B., Dahl-Jensen, D., Davies, S.M., Johnsen, S.J., et al., 2008. A 60,000 year Greenland stratigraphic ice core chronology. Climate of the Past Discussions 3, 47–57.
- Tan, L., Cai, Y., An, Z., Cheng, H., Shen, C., Gao, Y., Edwards, R.L., 2017. Decreasing monsoon precipitation in southwest China during the last 240 years associated with the warming of tropical ocean. *Climate Dynamics* 48, 1769–1778.
- Tan, L., Cai, Y., Cheng, H., Edwards, R.L., Gao, Y., Xu, H., Zhang, H., et al., 2018. Centennial-to decadal-scale monsoon precipitation variations in the upper Hanjiang River region, China over the past 6650 years. Earth and Planetary Science Letters 482, 580–590.
- Taylor, L.L., Leake, J.R., Quirk, J., Hardy, K., Banwart, S.A., Beerling, D.J., 2009. Biological weathering and the long-term carbon cycle: integrating mycorrhizal evolution and function into the current paradigm. *Geobiology* 7, 171–191.
- Terzer, S., Wassenaar, L.L., Araguásaraguás, L.J., Aggarwal, P.K., 2013. Global isoscapes for $\delta^{18}O$ and $\delta^{2}H$ in precipitation: improved prediction using regionalized climatic regression models. *Hydrology and Earth System Sciences* 17, 4713–4728.
- Treble, P., Fairchild, I.J., Griffiths, A., Baker, A., Meredith, K.T., Wood, A., McGuire, E., 2015. Impacts of cave air ventilation and in-cave prior calcite precipitation on Golgotha Cave dripwater chemistry, southwest Australia. *Quaternary Science Reviews* 127, 61–72.
- Treble, P., Shelley, J.M.G., Chappell, J., 2003. Comparison of high resolution sub-annual records of trace elements in a modern (1911–1992) speleothem with instrumental climate data from southwest Australia. *Earth and Planetary Science Letters* 216, 141–153.
- Voelker, A.H.L., 2002. Global distribution of centennial-scale records for Marine Isotope Stage (MIS) 3: a database. *Quaternary Science Reviews* 21, 1185–1212.

- Wagner, G., Beer, J., Masarik, J., Muscheler, R., Kubik, P.W., Mende, W., Laj, C., et al., 2001. Presence of the solar de Vries cycle (~205 years) during the last ice age. Geophysical Research Letters 28, 303–306.
- Wagner, J.D.M., Cole, J.E., Beck, J.W., Patchett, P.J., Henderson, G.M., Barnett, H.R., 2010. Moisture variability in the southwestern United States linked to abrupt glacial climate change. *Nature Geoscience* 3, 110–113.
- Wang, P., Wang, B., Cheng, H., Fasullo, J., Guo, Z., Kiefer, T., Liu, Z., 2014. The global monsoon across timescales: coherent variability of regional monsoons. *Climate of the Past* 10, 2163–2291.
- Wang, Q., Wang, Y., Shao, Q., Liang, Y., Zhang, Z., Kong, X., 2018. Millennial-scale Asian monsoon variability during the late Marine Isotope Stage 6 from Hulu Cave, China. *Quaternary Research* 75, 1–12.
- Wang, Y., Cheng, H., Edwards, R.L., An, Z., Wu, J., Shen, C., Dorale, J.A., 2001. A high-resolution absolute-dated late Pleistocene Monsoon record from Hulu Cave, China. *Science* 294, 2345–2348.
- Wang, Y., Cheng, H., Edwards, R.L., He, Y., Kong, X., An, Z., Wu, J., et al., 2005. The Holocene Asian monsoon: links to solar changes and North Atlantic climate. Science 308, 854–857.
- Wang, Y., Cheng, H., Edwards, R.L., Kong, X., Shao, X., Chen, S., Wu, J., et al., 2008. Millennial- and orbital-scale changes in the East Asian monsoon over the past 224,000 years. *Nature* 451, 1090–1093.

- Wolff, E.W., Chappellaz, J., Blunier, T., Rasmussen, S.O., Svensson, A., 2010. Millennial-scale variability during the last glacial: the ice core record. *Quaternary Science Reviews* 29, 2828–2838.
- Wu, H., Zhang, X., Li, X., Li, G., Huang, Y., 2015. Seasonal variations of deuterium and oxygen-18 isotopes and their response to moisture source for precipitation events in the subtropical monsoon region. *Hydrological Processes* 29, 90–102.
- Zhang, J., Jia, Y., Lai, Z., Long, H., Yang, L.H., 2011. Holocene evolution of Huangqihai Lake in semi-arid northern China based on sedimentology and luminescence dating. *Holocene* 21, 1261–1268.
- Zhao, K., Wang, Y., Edwards, R.L., Cheng, H., Liu, D., 2010. High-resolution stalagmite δ¹⁸O records of Asian monsoon changes in central and southern China spanning the MIS 3/2 transition. Earth and Planetary Science Letters 298, 191–198.
- Zhao, K., Wang, Y., Edwards, R.L., Cheng, H., Liu, D., Kong, X., Ning, Y., 2016. Contribution of ENSO variability to the East Asian summer monsoon in the late Holocene. *Palaeogeography, Palaeoclimatology, Palaeoecology* 449, 510–519.
- Zhou, H., Chi, B., Michael, L., Zhao, J., Yan, J., Alan, G., Feng, Y., 2008. High-resolution and precisely dated record of weathering and hydrological dynamics recorded by manganese and rare-earth elements in a stalagmite from central China. *Quaternary Research* 69, 438–446.